# Effect of citric acid quantity on LaAlO₃ formation in sol-gel synthesis with combustion

Kristina Antropova [a] *, Ruslan Kuzmin [a], Natalia Alexandrova [a],
Alexander Yurgin [a], Julia Malyutina [ab], Nomina Burkhinova [a]

**a:** Novosibirsk State Technical University, Novosibirsk 630073, Russia
**b:** Lavrentyev Institute of Hydrodynamics SB RAS, Novosibirsk 630090, Russia
**\*** Corresponding author: antropova.2017@stud.nstu.ru

## Abstract

Lanthanum aluminate (LaAlO₃) was synthesized using the nitrate-citrate sol-gel method followed by the combustion process. The synthesis was conducted using fuel-lean at pH 7, with metal precursor to citric acid mass ratios (Me:$C_6H_8O_7$) of 1:0.25, 1:0.37, and 1:0.48. The resultant products were analyzed using X-ray diffraction and scanning electron microscopy (SEM). After post-annealing at 900 °C, the formation of crystalline LaAlO₃ was confirmed, whereas the as-pyrolized product was found to be X-ray amorphous. It was established through thermal analysis that nitrate-citrate complexes decompose in several stages, and LaAlO₃ crystallizes at around 840 °C. An increase in citric acid concentration correlated with a reduction in microstress levels and a decrease in the size of coherent scattering regions, in agreement with the particle size measurement results obtained from SEM images. The synthesized nanoscale particles exhibited an average size in the range of 50–60 nm and a specific surface area greater than 15 m²/g. The synthesized powders were characterized by fragile porous aggregates composed of thin porous walls. Notably, an increase in citric acid concentration promoted the enlargement of pores within the aggregates while simultaneously reducing the pore size within the thin walls. Furthermore, the materials synthesized from the solutions with pH 1 demonstrated a larger average particle size (~75 nm) and smaller pore sizes, with combustion occurring at lower temperatures compared to the samples obtained from the solutions at pH 7.

## Key findings

● Lanthanum aluminate crystallises at 900 °C after combustion of fuel-lean in nitrate-citrate synthesis.

● Increasing the amount of fuel leads to the formation of a more developed porous system of aluminate aggregates.

● An inverse relationship between the amount of fuel and the particle size is observed.

## 1. Introduction

The investigation of aluminates has garnered significant attention in the scientific community. Among these compounds, lanthanum monoaluminate (LaAlO₃) stands out as a notable example [1]. LaAlO₃ is classified within the perovskite family. Notably, LaAlO₃ exhibits a cubic perovskite structure characterized by the space group Pm-3m. This compound is known to readily undergo a phase transition to a distorted rhombohedral perovskite structure, identified by the space group R-3c [2].

The interest in lanthanum aluminate (LaAlO₃) arises from its diverse functional properties. Doping LaAlO₃ with various cations further extends its range of application. It was reported [3] that the crystal structure of perovskite can include more than 90% of the elements of the periodic table. The dielectric properties, unique crystal structure characteristics and specific thermal expansion coefficients of LaAlO₃ facilitate its use in the fabrication of resonators and conducting films for microwave devices [4], as well as thermistors, which are resistors whose resistance decreases as temperature increases [5]. The

article [6] shows that for samples sintered at 1200–1400 °C, the coefficient of thermal expansion ranges from $5.5 \cdot 10^{-6}$ to $6.5 \cdot 10^{-6}$ $K^{-1}$, and the thermal conductivity ranges from 2.2 to 3.4 W/(m·K). In the field of catalysis, $LaAlO_3$ demonstrates potential due to its ability to produce materials with high surface area, along with notable chemical, thermal, and mechanical stability, as well as catalytic activity [7,8]. Additionally, the utility of aluminates in forming hexaaluminates, such as $LaAl_{11}O_{18}$, presents opportunities for developing $\alpha$-$Al_2O_3$-based ceramics with enhanced fracture toughness [9]. Recent findings indicate that lanthanum aluminate is also suitable for application in solid oxide fuel cells (SOFCs) owing to its improved oxygen conductivity [10, 11]. Moreover, the luminescent and optical properties of doped $LaAlO_3$ warrant further exploration, as the material has potential applications in the production of displays, solid-state lasers, thermal sensors, and light-emitting diodes (LEDs) [12–14].

A substantial body of research, as reviewed in [1], focuses on the synthesis of lanthanum aluminate ($LaAlO_3$) via the solid-phase reaction of alumina ($Al_2O_3$) and lanthana ($La_2O_3$). However, this method is characterized by the requirement of high reaction temperatures exceeding 1100 °C [3, 15]. The resultant particles tend to be large, which adversely affects their sintering ability and overall material properties. It is particularly noted that these drawbacks are pronounced when using inert precursors, such as $\alpha$-$Al_2O_3$. In [1,15], various methods for the preparation of highly dispersed $LaAlO_3$ powders are discussed. These methods include co-deposition, hydrothermal and solvothermal synthesis, mechano-synthesis, combustion, and the Pechini process [16]. Each technique offers distinct advantages and may mitigate the limitations associated with high-temperature solid-state synthesis.

Significant attention is directed toward the synthesis of $LaAlO_3$ via the sol-gel method with subsequent combustion. This approach encompasses several key steps: the mixing of precursor chemicals, the formation of a sol and subsequent gel, and thermal treatment to remove organic and volatile substances. The advantages of the sol-gel method include ease of scale-up, high product purity, straightforward doping processes, and a high specific surface area of the resultant powders [15]. For example, Mizukami et al [19] demonstrated that materials synthesized through sol-gel method exhibit a larger surface area compared to those produced via co-deposition. This observation holds true for heat treatments conducted up to 1100 °C; however, above this temperature, the specific surface area diminishes to below 60 m²/g. In study [17] powders obtained at 700 and 800 °C were reported to have surface areas of 43 and 35 m²/g, respectively. Additionally, the author noted that the materials synthesized by the sol-gel method exhibited superior sinterability and enhanced reactivity when compared to commercially available powders, such as $LaAlO_3$ from Alfa Aesar, which has an average surface area of only 4.6 m²/g.

The sol-gel method offers numerous advantages, particularly due to its wide array of synthesis parameters. By changing these parameters, researchers can readily obtain desired outcomes. Variations in these parameters have led to the customization of method names, which often reflect the composition of the gel-forming or fuel components. Common nomenclature includes terms such as citrate [20], glycine-nitrate [21], and glycol precursor method [22]. A variety of fuels have been employed in the synthesis of $LaAlO_3$: citric acid, urea, polyvinyl alcohol, glycine, and oleic acid [23, 24]. Numerous studies have focused on analyzing the efficiency of these fuel mixtures. For instance, Aruna et al [25] reported an enhancement in particle dispersibility when using a mixture of urea and glycine as a propellant, compared to materials synthesized when urea alone. Additionally, Chandradass and Kim [26] investigated the combust of varying ratios of citric and oxalic acids in their synthesis. Their findings indicated that $LaAlO_3$ produced using a combination of 0.0025 M citric acid and 0.0075M oxalic acid exhibited the smallest crystallite size, measuring 23.6 nm. The researchers concluded that utilizing a mixture of fuels not only reduces the exothermicity of the combustion reaction but also significantly decreases the crystallite size of the resultant material.

Currently, the most common chelating agent is citric acid. This is due to its acidic properties and its ability to form strong complexes with many compounds. Frequently, it is added in excess, with molar ratios of citric acid to cations ranging from 1 to 3 [15]. The formation of complexes, called citrates, also occurs in acidic medium. However, the process of co-complex formation can be accelerated by adjusting the pH (neutralization) using ammonia solution. Then the formation of complexes occurs in reactions with hydroxides [27]. In addition to stimulating the complexation reaction, the formation of ammonium nitrate occurs in the systems. It also acts as an oxidant in the exothermic redox process [28]. It was reported in [10] that the average crystallite size decreases with increasing pH of the initial solution. The calculated values at pH 2, 7 and 9 were 35, 31 and 29 nm, respectively.

**Table 1** A brief analysis of $LaAlO_3$ synthesis methods (adapted from [3, 15, 17, 18]).

| Synthesis method | Surface area (m²/g) | Particle size, nm | Purity | Temperature of crystallization, °C |
|---|---|---|---|---|
| Solid-state reaction | <2.5 | >1000 | low | >1100 |
| Co-precipitation | 4.5–20 | >10 | high | 800 |
| Microwave assisted method | 1–36 | >100 | excellent | 600–800 |
| Hydro- and solvothermal synthesis | 50 | >100 | very high | No calcination |
| Mechanosynthesis | <13 | >50 | high | No calcination |
| Sol–gel | 5–20; <43 | >10 | excellent | 600–1000 |

This study investigates the phase composition, aggregate morphology, and particle size of lanthanum aluminate (LaAlO$_3$) synthesized through a nitrate-citrate sol-gel combustion method utilizing low-concentration precursor solutions. The sol-gel combustion technique is selected for its ability to produce high-purity powder with tunable functional properties by systematically varying synthesis parameters. Our findings reveal that LaAlO$_3$ can be effectively crystallized at relatively low temperatures, resulting in particle sizes that demonstrate potential applicability in various technological fields, including catalysis, photonics, and solid oxide fuel cells. The insights gained from this research are crucial for optimizing the synthesis of lanthanum aluminate and enhancing its functional applications.

## 2. Materials and methods

### 2.1. Synthesis of LaAlO$_3$ powders

Lanthanum aluminate was synthesized using the citrate method, employing La(NO$_3$)$_3$·6H$_2$O (Vekton, Russia, 99.9% purity) and Al(NO$_3$)$_3$·9H$_2$O (Vekton, Russia, 98% purity) as the initial precursors in a 1:1 molar ratio. The salts were completely dissolved in a small amount of distilled water and 0.5 M solutions were prepared. Upon mixing the nitrate solutions at ambient temperature, a citric acid solution (C$_6$H$_8$O$_7$), prepared in a similar manner, was added with continuous stirring using a magnetic stirrer (Tagler MM 135 H). The mass ratios of metal precursors to citric acid (Me:C$_6$H$_8$O$_7$) was varied as follows: 1:0.25 (composition 1); 1:0.37 (composition 2); 1:0.48 (composition 3).

The pH of the resulting solutions was adjusted to maintain stability and prevent precipitation by the gradual addition of concentrated NH$_4$OH, aiming for a target pH of 7–8. Additionally, a fourth composition (composition 4) with a precursor-to-citric acid ratio of 1:0.48 was synthesized without pH adjustment, omitting NH$_4$OH. The pH levels of the nitrate solutions and their mixtures exhibited a pH of 1. Upon the introduction of NH$_4$OH, the pH stabilized at 7–8. Notably, the transparent solution transitioned to a white coloration between pH 2–4 before returning to transparency; this behavior was not observed in the material with the lowest citric acid content. At pH 7–8, the solution retained a whitish appearance, likely due to the precipitation of hydroxides.

Mixing of the final solutions was conducted for two hours at a maximum temperature of 60 °C. Subsequently, water was evaporated using a heating apparatus maintained at temperatures not exceeding 270 °C, resulting in the formation of a clear gel. The dried products primarily formed charred powders, with the exception of the material synthesized without pH adjustment. These powders were then subjected to heat treatment. Initially placed in a preheated oven at 250 °C, the temperature was rapidly increased to 400 °C before the samples were cooled in ambient air. A volumetric expansion was observed during reactions occurring near 300 °C, while the powders retained a

black-grey coloration. After cooling, the powders were finely ground and underwent annealing at 900 °C, followed by slow cooling within the oven EKPS-10, resulting in a final product characterized as a white fluffy powder. Additionally, the precursors were heat treated at 700 and 800 °C.

It is worth noting that milling of the materials at various synthesis stages was not conducted. Instead, the aggregates formed from the powder products post-combustion and during annealing at 900 °C disintegrated naturally during handling.

### 2.2. Characterisation

The calculation of redox reactions to determine the richness ($\phi_e$<1) or leanness ($\phi_e$>1) of the fuel-oxidizer mixtures was carried out using equation 1 [29]. The valencies of the oxidizing elements N and O were taken as +5 and +2, respectively. The valences of fuel elements C and H were taken as –4 and –1 respectively. The valences of Al and La were considered neutral.

$$\phi_e = p/r, \tag{1}$$

where $p$ – the sum of the coefficients of oxidizing elements in specific formula valence; $r$ – the sum of the coefficients of reducing elements in specific formula valence multiplied by (–1).

The thermal decomposition of the dried precursor was carried out using a STA7300 thermal analyzer (Hitachi). The samples were heated from 25 to 1000 °C at a heating rate of 15 °C/min.

The phase composition was determined using X-ray diffraction patterns obtained on an ADVIN POWDIX 600 diffractometer using the PDF-4 database. The imaging was performed in Cu Kα radiation (λ(Kα1) = 1.540562 Å) in the angle range from 20 to 70° in steps of Δ2θ = 0.01°. The lattice parameter and X-ray density were calculated using Profex software (version 5.3.1) [30]. Similar to [31] the microstress level and the size of the coherent scattering regions were estimated using the Williamson-Hall equation:

$$\beta_{hkl}·\cos\theta = 0.9·\lambda/D+4\varepsilon·\sin\theta \tag{2}$$

where $\beta_{hkl}$ – the full width at half maximum intensity for various diffraction planes; θ – the angular position of the reflex, in radians; λ – the wavelength of the incident radiation, in nm; $D$ – the average size of the crystallites, in nm; ε – the microstress [32].

Preliminary analysis of the obtained powders was carried out on ADF X100 stereomicroscope. The size and morphology of powder particles, aggregates and pores were studied on a Merlin scanning electron microscope in the secondary electron mode. The samples were coated with a gold layer to improve the conductivity. The measurements were performed using JMicroVision software (version 1.3.4) [33] and DLgram01 cloud service [34].

The specific surface area of the synthesized powders was measured using a Sorbi-MS according to the BET technique at relative partial pressures of 0.06, 0.09, 0.15, and

$0.20$ $P/P_0$. A SorbiPrep station was used to degas the samples before measuring their specific surface area. Heating was carried out up to 200ºC, with a holding time of 40 min. The particle size $D_{BET}$ (nm) was calculated from the specific surface area data using the equation:

$$D_{BET} = 1000 \cdot K/(\rho \cdot S) \qquad (3)$$

where $K$ is the particle shape coefficient ($K = 6$ for spherical particles); $S$ is the surface area of a powder, in $m^2/g$; $\rho$ is the theoretical density of $LaAlO_3$, in $g/cm^3$.

## 3. Results and Discussion

### 3.1. Oxidation-reduction ratio of mixtures. Thermal analysis

The onset temperatures for combustion and the subsequent flame temperatures are influenced by the fuel mixture and the fuel-to-oxidant ratio. This in turn determines the surface area, size distribution and agglomeration of particles in the resultant material [25, 26]. The calculations were carried out using equation 1, and it was found that the mixtures prepared are lean. Specifically, the ratio of oxidant to reducing agent exceeds 1, deviating significantly from the stoichiometric ratio as the concentration of citric acid is diminished. Notably, combustion is nonetheless observed, resulting in the formation of fluffy powders.

The residues within the crucibles, after heat treatment of the dried gels at 400 ºC, were examined using a stereomicroscope (Figure 1). The most pronounced volumetric effect was noted in materials with a metal to citric acid ($Me:C_6H_8O_7$) ratio of 1:0.48. A reduction in this ratio corresponded with a diminished volumetric effect. For a $Me:C_6H_8O_7$ ratio of 1:0.25, no significant volumetric effect was evident; the inner surface of the crucible appeared uniformly coated with fine black particles. Considering that the amounts of $La(NO_3)_3 \cdot 6H_2O$ and $Al(NO_3)_3 \cdot 9H_2O$ remained constant, the observed phenomena can be attributed solely to the varying quantities of citric acid incorporated into the mixtures.

In our research, heating pH-regulated materials on a laboratory hot plate to 270 ºC did not reach the necessary temperatures to initiate combustion. In contrast, the pH-unregulated material exhibited swelling during the drying process, producing brown-colored smoke, which can be attributed to the release of $NO_2$ [25]. These observations highlight the critical role of synthesis conditions on the combustion behavior and thermochemical dynamics of $LaAlO_3$.

In the research by Yagodina and Mishenina [35], $LaAlO_3$ powder was synthesized using the nitrate-citrate method, maintaining a stoichiometric oxidant-fuel ratio with citric acid and aluminate-forming compounds in a 1:1 ratio. Thermal analysis results indicated that exothermic combustion processes occurred within the temperature range of 350–475 ºC, primarily due to the oxidation of metal-citrate complexes, which was accompanied by significant

mass loss. The authors noted a substantial activation energy of 600 kJ/mol associated with these reactions.

Further investigations by Lee et al [20] revealed the presence of exothermic peaks beginning at 400.2 ºC during the gelling of an aqueous solution of aluminum nitrate and citric acid at varying ratios. It was observed that when the nitrate-to-citric acid ratio was between 0.1 and 0.33, the decomposition process occurred in two distinct stages. However, increasing the citric acid ratio beyond 0.33 resulted in a three-stage decomposition process, with the temperatures of subsequent decomposition steps rising correspondingly with the increasing citrate-to-nitrate ratio.

For powders with the lowest volumetric effect (for which $Me:C_6H_8O_7$ is 1:0.25 and 1:0.48 without $NH_4OH$) the thermal analysis was performed. The curves of thermogravimetry and differential thermal analysis (TG/DTA), and derivative thermogravimetry analysis (DTG) are shown in Figure 2.

Endothermic processes from the beginning of heating are explained by the loss of adsorbed and bound water and the removal of light organic compounds. Up to about 300 ºC, endothermic effects can also be associated with the decomposition of hydroxides [22]. The weight losses at this stage are about 16.5 and 13.2% for materials 1:0.48 and 1:0.25, respectively.
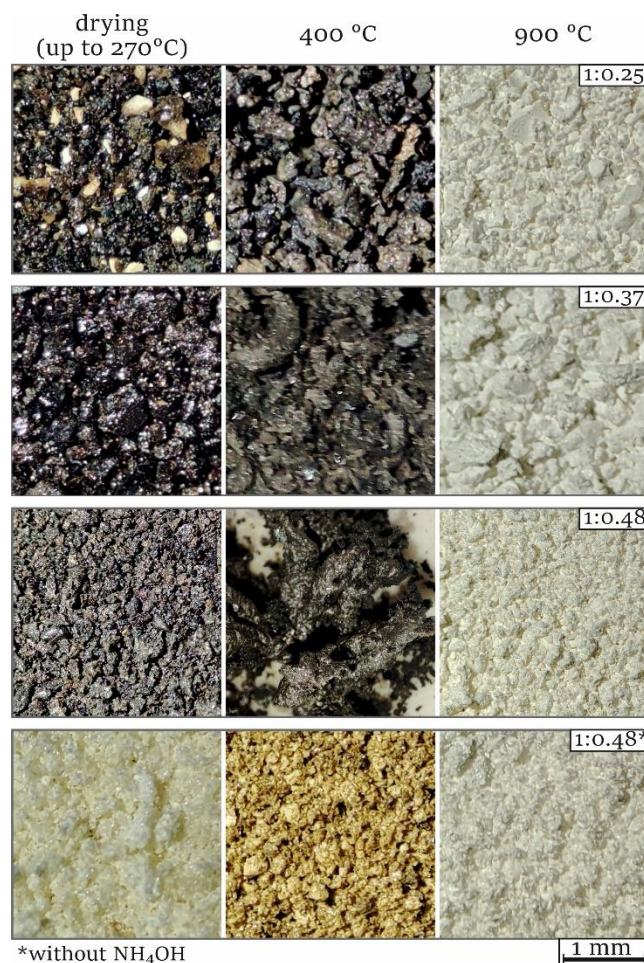


**Figure 1** Appearance of the products of the nitrate-citrate synthesis at different oxidant and reductant ratios, processed at various temperatures.

Exothermic processes that were recorded are associated with the oxidation of nitrate-citrate complexes. For a material with a ratio (Me:$C_6H_8O_7$) of 1:0.48 without $NH_4OH$, two stages can be distinguished with maxima at 403.3 and 423.8 °C. At these temperatures, decomposition of unreacted citric acid and nitrate-citrate complexes (combustion) occurs [36]. Since citric acid is not used in excess, more complete reactions of the formation of nitrate citrate complexes can be facilitated by increasing the mixing time or by increasing the mixing temperature. The weight loss during this stage was 34.7%. For a material with a ratio (Me:$C_6H_8O_7$) of 1:0.25, several exothermic reactions occur. These may be related to the decomposition of nitrate-citrate complexes (433.9 °C), citric acid (372.3 °C) and other compounds (310.9 °C), for example, hydroxycarbonates [20]. The presence of the latter reaction for this composition can be explained by contamination of the starting powder with carbon, which is not typical for material with ratio (Me:$C_6H_8O_7$) of 1:0.48 without $NH_4OH$ (Figure 1). The total weight loss in this temperature range was 50%.

Exothermic effects near 840 °C are associated with the crystallization of $LaAlO_3$ [37]. Total weight losses were 56.4 and 67.8% for materials with ratios (Me:$C_6H_8O_7$) 1:0.25 and 1:0.48 without $NH_4OH$, respectively.

## 3.2. X-ray phase analysis

Figure 3 presents the X-ray diffraction patterns of the resultant and intermediate materials. All resultant powders (diffractograms e-h) treated at 900 °C correspond to lanthanum monoaluminate ($LaAlO_3$, R-3c (167)). No reflection associated with the parent or intermediate compounds are observed, indicating complete conversion of the reaction. Notably, in the materials with a metal to citric acid (Me : $C_6H_8O_7$) ratio of 1:0.25, a shift in the peak positions and a change in the signal-to-noise ratio are detected. This phenomenon may stem from processes related to pH adjustment or incomplete crystallization.

The diffractograms of the dried gel (diffractogram a) and the combustion products (diffractogram b) are also illustrated in Figure 3. The results are presented for materials with metal precursor to citric acid mass ratios of 1:0.48, 1:0.37, and 1:0.25. Regardless of these ratios, all compositions exhibit similar diffraction patterns indicative of an amorphous state (Figure 3, diffractogram a, b). The materials annealed at 700 and 800 °C (diffractograms c and d) are predominantly amorphous; however, the appearance of low-intensity reflection can be observed, which indicates the beginning of crystallization. This is consistent with the results of thermal analysis described in Section 3.1. The onset of crystallization at a lower temperature than determined by the TG-DTA curves is associated with a lower heating rate, the accuracy of maintaining the set temperature, and the temperature gradients within the furnace.
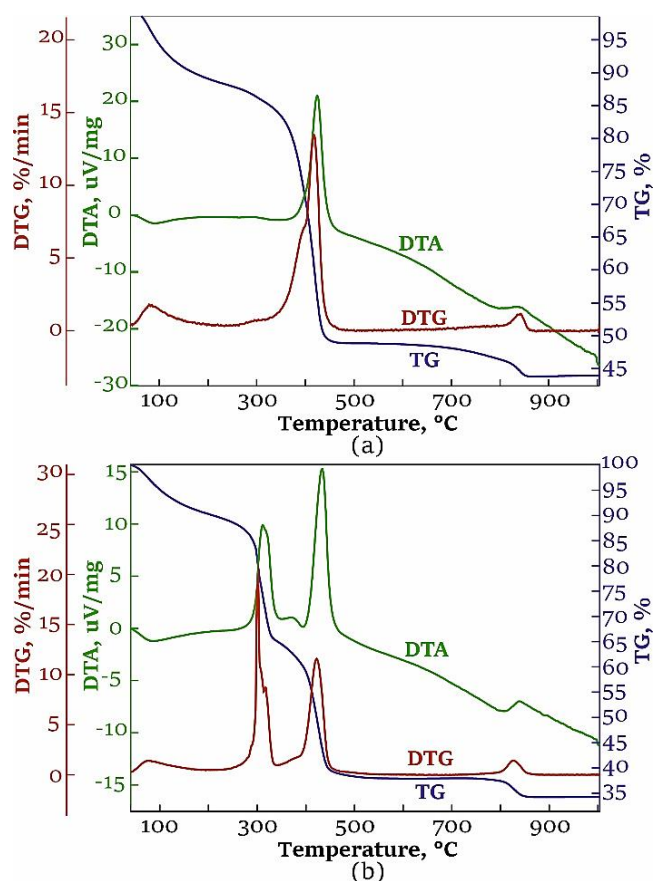


**Figure 2** TG-DTA-DTG curves of the dried gel with ratio (Me:$C_6H_8O_7$) 1:0.48 without $NH_4OH$ (a) and 1:0.25 (b).
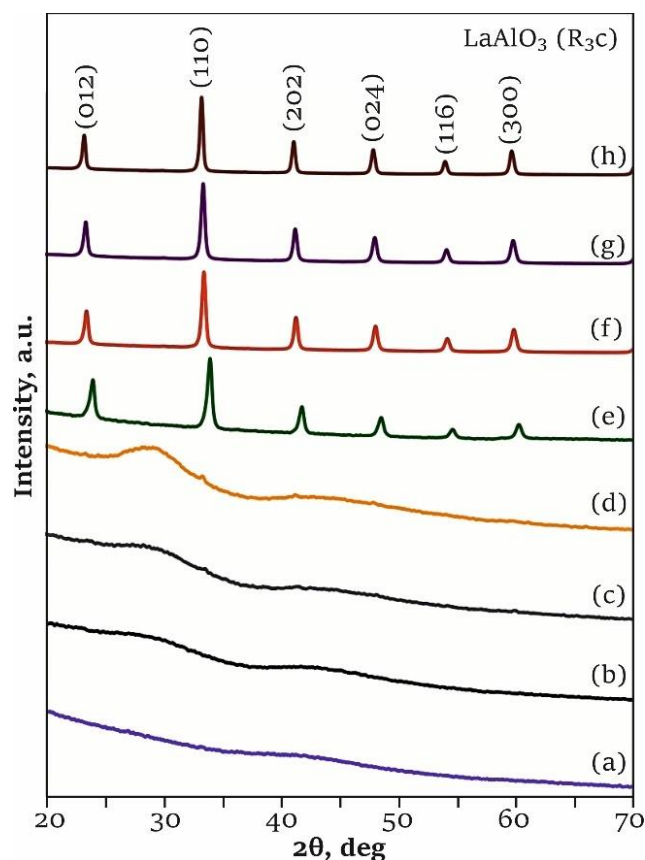


**Figure 3** Diffraction patterns of the obtained powders after drying (a); after heating to 400 °C (b); materials after annealing at 700 °C (c), 800 °C (d), 900 °C with a ratio of 1:0.25 (e); 1:0.37 (f); 1:0.48 (g); 1:0.48 without $NH_4OH$ (h).

Similar results were reported in the literature [26, 38]. Zhang et al [5] demonstrated that LaAlO$_3$ forms at 800 °C regardless of the Me:C$_6$H$_8$O$_7$ ratio, which includes 1:1, 1:1.5, 1:2, and 1:3. Their research indicates that the pH of the solution significantly influence the synthesis process; aluminate is produced at 800 °C at pH of 4, while crystallization initiates at 600 °C when the pH is 9. They observed that an alkaline environment facilitates a reduction in the synthesis temperature. Conversely, another study [39] indicates that further washing and grinding of intermediate products, along with the synthesis of a homogeneous gel, can lower the formation temperature of LaAlO$_3$ to 600 °C.

Table 2 presents a summary of the results obtained from X-ray diffraction analysis performed using Profex software (version 5.3.1). The calculated microstresses and sizes of coherent scattering regions are shown in Figure 4. The crystallite size (CS) and microstresses (MS) were determined on linear fitting data, using the Y-axis intersection for CS and the slope magnitude on the X-axis for MS, in accordance with Equation 2.

The highest measurement error is observed in the material with minimum amount of citric acid. Additionally, the lattice parameters of this material, along with the level of microstresses, are significantly elevated compared to others. This phenomenon is likely attributed to the retention of the amorphous component of the material, as no alloying processes were undertaken that could exert this influence. The authors of [40] noted that variations in lattice strain, whether an increase or decrease, can be correlated with changes in dislocation density. The observed positive slope of the linear curves signifies lattice expansion within the nanoparticles. Notably, a correlation is observed between the heightened values of the lattice parameter, crystallite size, and microstress levels.

## 3.3. SEM-Analysis

The morphology of LaAlO$_3$ powder materials obtained by sol-gel method followed by combustion was analyzed using a scanning electron microscopy. Figure 5 shows a comparison of materials in which Me:C$_6$H$_8$O$_7$ was 1:0.48, when obtained without and with pH adjustment. After heating on the hot plate (up to 270 °C), the particle aggregates of the material with unregulated pH are friable and porous (Figure 5 a). This indicates that combustion occurred already at this preparation stage. At these temperatures, this effect is not observed in the second material (Figure 5 b), indicating insufficient heating.
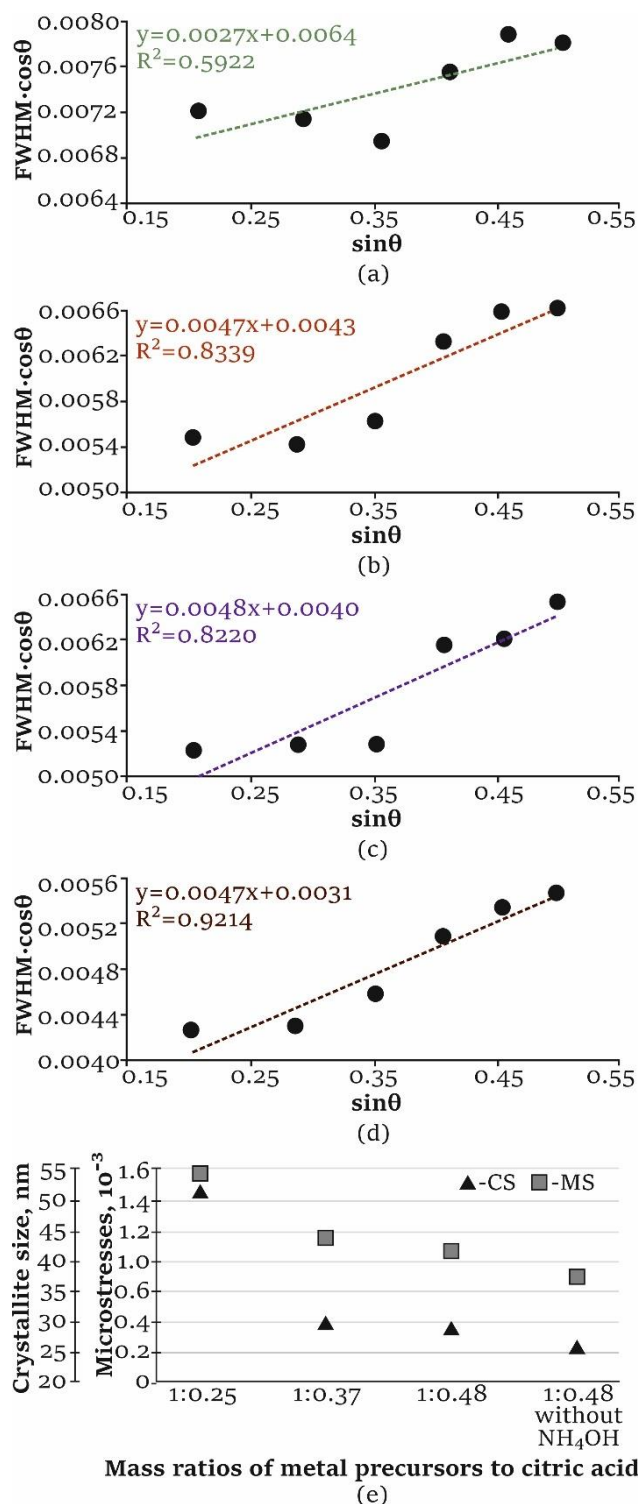


**Figure 4** Williamson-Hall dependences calculated from diffractograms of synthesized powders with ratio (Me:C$_6$H$_8$O$_7$) 1:0.25 (a); 1:0.37 (b); 1:0.48 (c); 1:0.48 without NH$_4$OH (d); and dependencies of CS and MS on the ratio of components (e).

**Table 2** Dependence of lattice parameters and X-ray density on the ratio of components.

| | Ratio Nitrates:C$_6$H$_8$O$_7$ | Lattice parameter | | X-ray density | Refinement quality parameters | |
|---|---|---|---|---|---|---|
| | | a, Å | c, Å | | Rwp | GOF |
| 1 | 1:0.25 | 5.36739±0.00032 | 13.14592±0.00089 | 6.497 | 4.34 | 1.49 |
| 2 | 1:0.37 | 5.36403±0.00006 | 13.13884±0.00024 | 6.509 | 2.39 | 1.42 |
| 3 | 1:0.48 | 5.36435±0.00005 | 13.13956±0.00021 | 6.508 | 2.35 | 1.34 |
| 4 | 1:0.48[a] | 5.36417±0.00006 | 13.13685±0.00014 | 6.507 | 2.32 | 1.35 |

[a] without pH adjustment.
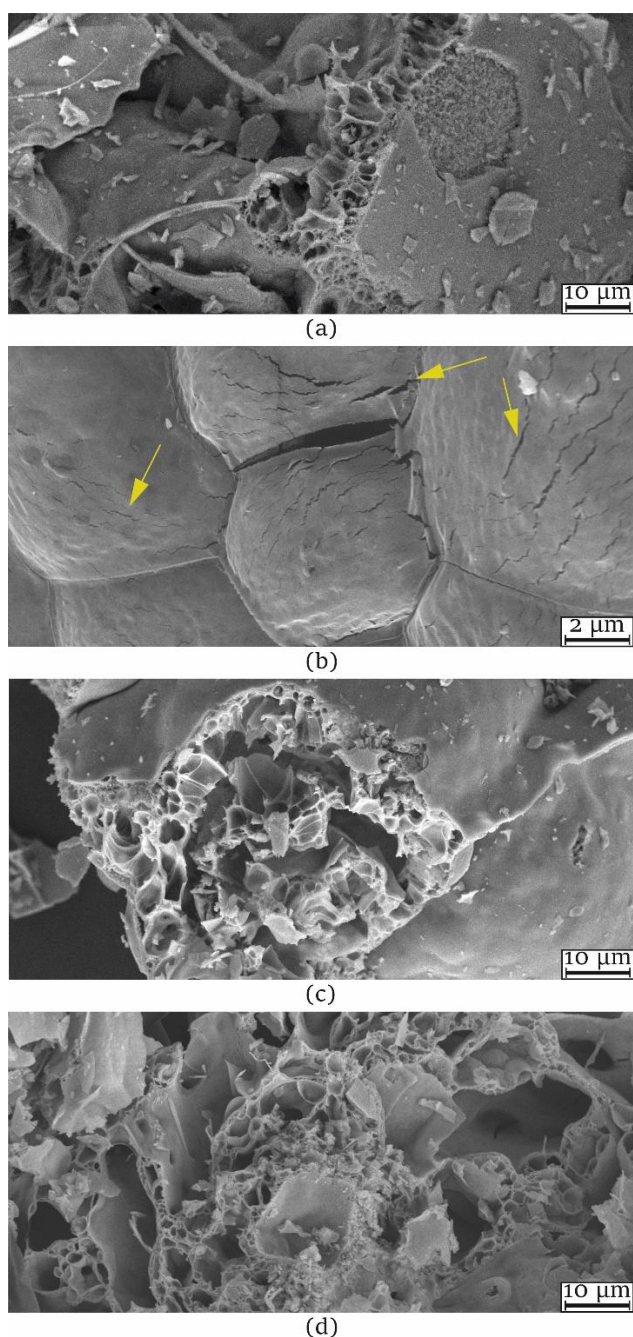
**Figure 5** Morphology of aggregates of materials with a ratio of 1:0.48 obtained by heating to 270 °C without $NH_4OH$ (a) and with $NH_4OH$ (b); at 400 °C without $NH_4OH$ (c) and with $NH_4OH$ (d).

The presence of cracks on the surface of the particles indicates the beginning of a reaction accompanied by an increase in volume. After heating up to 400 °C, the morphology of particles of both materials looks the same (Figure 5 d, c). At the same time, no visible volume effect was observed for the material without pH adjustment. It can be concluded that materials obtained from solutions with pH 7–8 require higher temperatures to initiate combustion.

The powders were subjected to natural milling resulting in a broad distribution of aggregate sizes following annealing at 900 °C, spanning from a few micrometers to several hundred micrometers. The average agglomerate size for the sample without $NH_4OH$ was determined to be 25 μm. In contrast, for the materials with adjusted pH, the average aggregate sizes ranged from 55 to 70 μm, contingent upon the decreasing concentration of citric acid. This trend can be attributed to the fact that a higher concentration of citric acid facilitates more vigorous combustion, leading to a significant volumetric effect. Consequently, the aggregates formed under these conditions exhibit increased porosity and are more amenable to fragmentation.

Figure 6 illustrates the structural characteristics of the powders post-annealing at 900 °C, alongside the corresponding particle size distributions. The average particle size ($d_{ave}$) measured from SEM-images of the material without $NH_4OH$ was 75±1 nm. For the pH-adjusted materials, the average particle size measured from SEM-images varied as follows with decreasing citric acid concentration: 55±1 nm for the first sample, 55±1 nm for the second, and 60±1 nm for the sample with the minimum amount of citric acid. The observed increase in average particle size for the sample with the least citric acid is likely a result of the loss of finer particles. As detailed in Section 3.1, the smaller particles settled uniformly on the surface of the crucible, rendering them inaccessible for subsequent analysis.

Zhang et al [5] demonstrated that citric acid concentration and pH do not significantly influence the average particle size of $LaAlO_3$ powders, which remains in the range of 24 to 30 nm. It can be noted that particle sizes measured from SEM images and those calculated from X-ray diffraction (XRD) patterns exhibit minor discrepancies. This variation can be attributed to the fact that X-ray intensity is proportional to the average particle volume, whereas SEM measurements focus on the average particle diameter. Furthermore, the authors report that increasing the amount of water during synthesis contributes to a reduction in particle size. In a related study, it was observed that slight deviations in particle size uniformity and distribution are linked to imbalances in heat and mass transfer throughout the synthesis process [12].

The results of measuring the specific surface area of synthesized powders and the calculated particle size of $D_{BET}$ are shown in Table 3. The calculated particle sizes differ from those measured by SEM images by no more than 6 nm. Similarly, Tian et al. [41] reported a 7 nm particle size difference ($D_{BET}$ = 93 nm and $D_{TEM}$ = 100 nm). This size difference is related to the shape of the particles and the presence of connections between them. The specific surface area for all materials exceeds 15 $m^2/g$. The high specific surface area is explained by the multistage release of gas products during decomposition, preventing agglomeration of synthesized powder [17].

During the combustion process, aggregates exhibiting a developed porous structure are formed. Kumar et al. [12] characterized this structure as spongy and porous, attributing its formation to the significant release of gases such as $CO_2$, CO and $N_2$ during the synthesis process. The materials synthesized in our study exhibit a similar morphology. Specifically, thin porous walls of nanoscale particles align such that extensive cavities of irregular rounded shapes are created between them (see Figure 7 a).
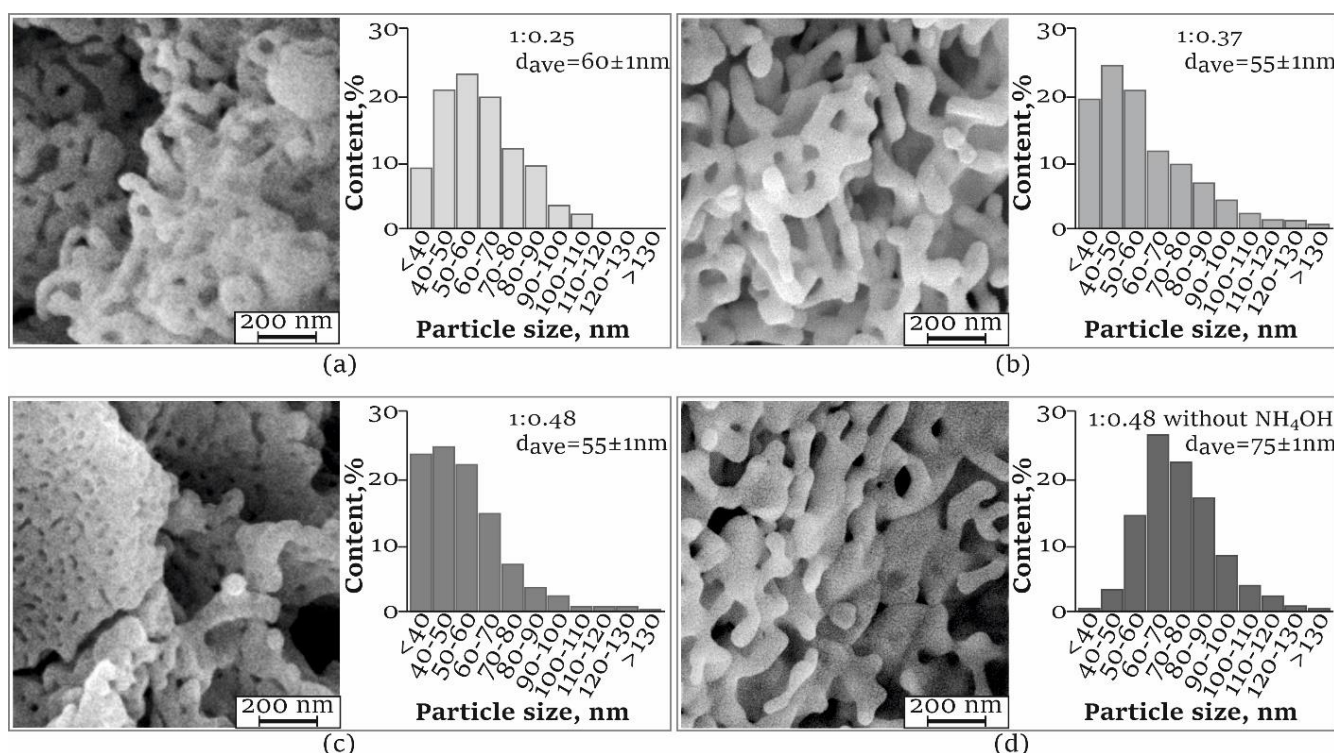
**Figure 6** Morphology and particle size distribution after annealing at 900 °C of materials with a ratio of 1:0,48 without NH$_4$OH (a) and with NH$_4$OH (b); 1:0.37 (c) and 1:0.25(d).

**Table 3** BET specific surface area and DBET.

| Ratio Nitrates : C$_6$H$_8$O$_7$ | BET, m²/g | $D_{BET}$, nm |
|---|---|---|
| 1:0.25 | 16.2 | 60.3 |
| 1:0.37 | 16.6 | 55.2 |
| 1:0.48 | 15.2 | 55.6 |

The sizes of these cavities vary from a few tens of micrometers down to fractions of a micrometer. Notably, the number of the large cavities exceeding 9 μm in size is considerably lower, with their presence being negligible in materials synthesized with minimal citric acid concentrations.

For the material synthesized without pH stabilization, the average cavity size is 2.3±0.1 μm, with more than 75% of the cavities falling within the 1–3 μm range and no more than 5% measuring below 1 μm. Conversely, the material with equivalent composition but obtained under pH-stabilized conditions displays larger cavities, with an average size reaching 4.0±0.2 μm. The distribution of cavity sizes in the pH-stabilized material shows an equal prevalence (27%) of cavities measuring up to 1 μm and those in the 3–6 μm range. Moreover, a noteworthy proportion of cavities greater than 9 μm was recorded, accounting for approximately 10% of the total observed cavities.

The material synthesized with a Me:C$_6$H$_8$O$_7$ ratio of 1:0.25 exhibited the smallest average cavity size of 0.82±0.05 μm. In this case, over 75% of the cavities were smaller than 1 μm, with only 2% of the analyzed areas falling in the 3–6 μm range; voids larger than 6 μm were not detected in the scanning electron microscope images. These findings confirm the impact of citric acid concentration on the volume reaction degree during the combustion process.

Furthermore, the structural characteristics observed may correlate with the formation of a fractal structure during sol-gel processes, as described in the paper [42]. The pore distribution formed between the particles within the walls and the average pore size ($d_{ave}$) are illustrated in Figure 7 b-e. The most prevalent pore sizes range between 10 and 30 nm, with the exception of the material with minimal citric acid, where a significant proportion of pores exhibit sizes between 30 and 50 nm.

## 4. Limitations

This study conducted crystallization annealing exclusively at a temperature of 900 °C. It is well established that both the temperature and duration of the annealing significantly in-fluence the crystallinity of the resulting phase as well as the particle size. Consequently, further investigation is warranted to identify the minimum annealing temperature required to achieve the desired crystallinity of the synthesized compound.

Additionally, the synthesized powders were not subjected to further milling, which could have facilitated a more precise estimation of particle size. It is important to note that light nanoscale particles could not be entirely retrieved from the surfaces of crucibles and storage or transport vessels. The observed particles tend to form aggregates that are fused together, lacking discernible boundaries. This aggregation complicates the accurate measurement of particle sizes, thereby presenting a challenge to the characterization process.
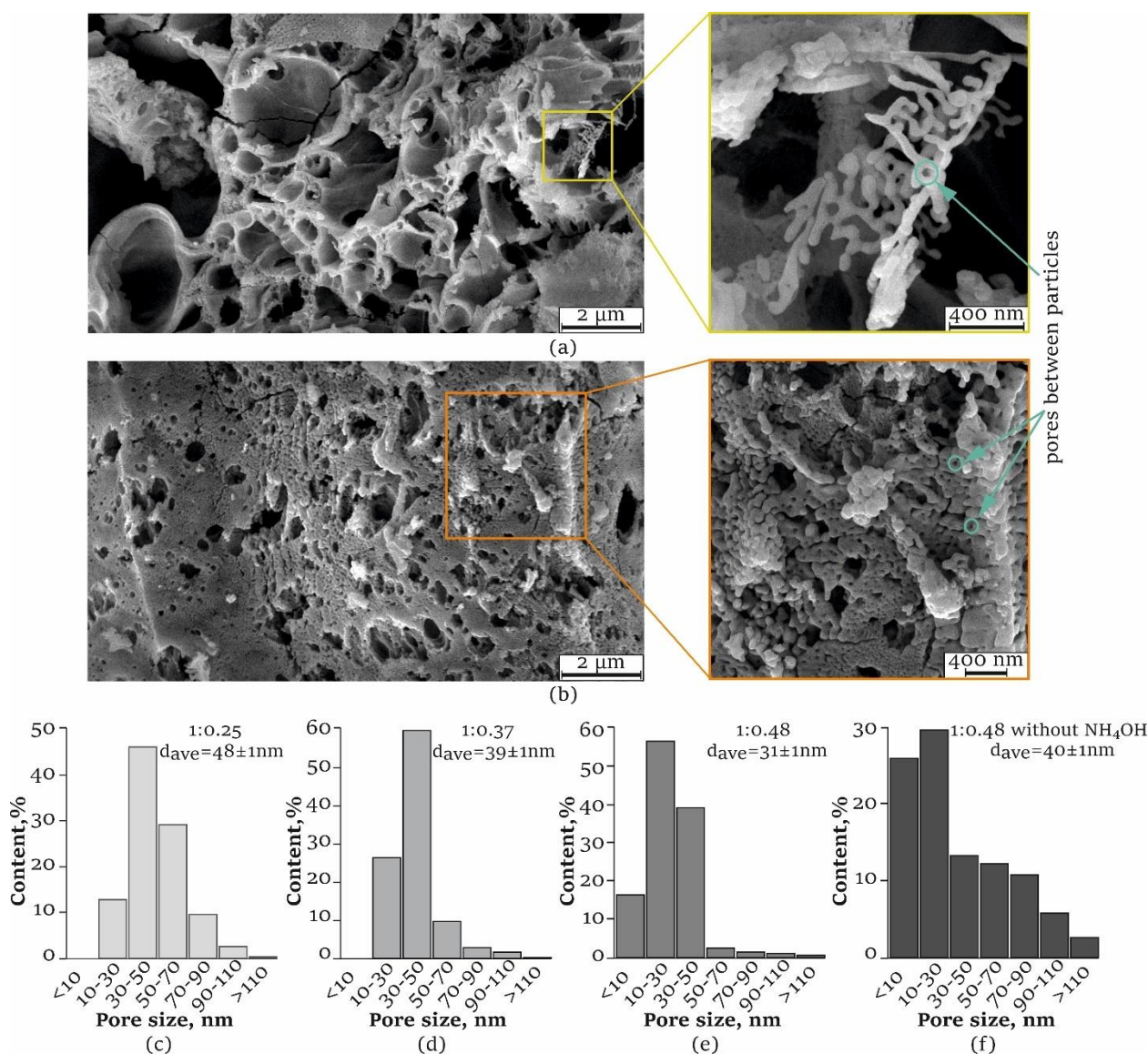
**Figure 7** Pore morphology (a, b) and pore size distribution between particles after annealing at 900 °C of materials with a ratio of 1:0.48 1:0,25 (c); 1:0,37 (d); 1:0,48 (e); 1:0,48 without NH$_4$OH (f).

## 5. Conclusions

In this study, nanoscale powders of LaAlO$_3$ synthesized using the nitrate-citrate sol-gel method followed by the combustion process. The prepared compositions, which incorporated varying amounts of citric acid, were classified as lean in terms of composition. An increase in citric acid concentration was found to enhance the volumetric effects of the reaction.

Thermal analysis methods showed that the decomposition of precursors occurs in several stages within the temperature range 300–450 °C. LaAlO$_3$ crystallizes at a temperature of about 840 °C for different compositions. The total weight loss is greater than 50%.

X-ray diffraction analysis revealed that the product remained amorphous after combustion and annealing at 400 °C. After annealing at 700 and 800 °C, weak LaAlO$_3$ reflections were detected, indicating the beginning of crystallization. Following annealing at 900 °C, the phase composition of the powder was confirmed to be LaAlO$_3$ (R-3c,

167). Additionally, as the amount of citric acid increased, microstress levels decreased from 0.0016 to 0.0010, while the average size of coherent scattering regions decreased from 51.4 to 28.9 nm. Notably, the changes in lattice parameters were observed to be non-linear and minimal.

The synthesized aggregates exhibited irregular shapes characterized by thin walls formed by intergrown, rounded particles. The cavities between these walls reached sizes of several micrometers, while the pore sizes within the walls predominantly ranged from 10 to 50 nm. As the concentration of citric acid (C$_6$H$_8$O$_7$) increased, the aggregate size decreased and the pore size increased, resulting in a reduction of the average particle size from 60 nm to 50 nm.

It was found that the specific surface area, determined using the BET method, is greater than 15 m²/g. The calculated particle sizes were close to the measured ones; the difference was less than 6 nm.

The preparation of LaAlO$_3$ with a Me:C$_6$H$_8$O$_7$ = 1:0.48, conducted without pH adjustment (pH = 1), yielded similar diffraction patterns. Observed effects and scanning

electron microscopy (SEM) images indicated that combustion occurred at lower temperatures relative to powders of similar composition synthesized at a pH of 7, which displayed an increase in average particle size (~70 nm) alongside a decrease in the size of aggregates and pores.

In conclusion, this study highlights the viability of synthesizing $LaAlO_3$ from lean mixtures, with and without pH adjustment, and demonstrates the influence of nitrate-citrate sol-gel synthesis conditions on the characteristics of the resultant powder products.

## Supplementary materials

No supplementary materials are available.

## Data availability statement

The raw/processed data required to reproduce the above findings cannot be shared at this time as the data also forms part of an ongoing study.

## Author contributions

Conceptualization: K.A., R.K.
Data curation: N.A., A.Yu.
Formal Analysis: A.Yu., K.A.
Investigation: Ju.M., N.A., K.A.
Methodology: R.K.
Validation: N.B., N.A.
Visualization: K.A., B.N.
Writing – original draft: K.A., R.K.
Writing – review & editing: K.A.

## Conflict of interest

The authors declare no conflict of interest.

## Additional information

Author IDs:
   Kristina Antropova, Scopus ID 57759105600;
   Ruslan Kuzmin, Scopus ID 57189894268;
   Natalia Alexandrova, Scopus ID 57216883212;
   Alexander Yurgin, Scopus ID 58024100900;
   Julia Malyutina, Scopus ID 56070653000;
   Nomina Burkhinova, Scopus ID 57886417900.

Website:
   Novosibirsk State Technical University, https://en.nstu.ru/;
   Lavrentyev Institute of Hydrodynamics SB RAS, https://www.hydro.nsc.ru/.

# References

1. Heveling J. La-Doped Alumina, Lanthanum Aluminate, Lanthanum Hexaaluminate, and Related Compounds: A Review Covering Synthesis, Structure, and Practical Importance. Ind Eng Chem Res. 2023;62:2353–86. doi:10.1021/acs.iecr.2c03007

2. Liu Z, Chen Q. Phase transition of $LaAlO_3$ nanocrystal enhanced optical linear&third order nonlinear and dielectric properties of glasses. J Non-Cryst Solids. 2023;599:121965. doi:10.1016/j.jnoncrysol.2022.121965

3. Royer S, Duprez D, Can F, Courtois X, Batiot-Dupeyrat C, Laassiri S, Alamdari H. Perovskites as Substitutes of Noble Metals for Heterogeneous Catalysis: Dream or Reality. Chem Rev. 2014;114(20):10292–368. doi:10.1021/cr500032a

4. Chandradass J, Kim KH. Synthesis and characterization of $LaAlO_3$ nanopowders by emulsion combustion method. J Alloys Compd. 2009;481:L31–4. doi:10.1016/j.jallcom.2009.03.072

5. Zhang X, Chu W, Bai H, Liang S. $LaAlO_3$: a new high-temperature negative temperature coefficient thermistor. J Mater Sci Mater Electron. 2022;33:12093–103. doi:10.1007/s10854-022-08169-x

6. Vourdas N, Marathoniti E, Pandis PK, Argirusis C, Sourkouni G, Legros C, Mirza S, Stathopoulos VN. Evaluation of $LaAlO_3$ as top coat material for thermal barrier coatings. Trans Nonferrous Met Soc China. 2018;28:1582–92. doi:10.1016/S1003-6326(18)64800-9

7. Lee G, Kim I, Yang I, Ha JM, Na HB, Jung JC. Effects of the preparation method on the crystallinity and catalytic activity of $LaAlO_3$ perovskites for oxidative coupling of methane. Appl Surf Sci. 2018;429:55–61. doi:10.1016/j.apsusc.2017.08.092

8. Moothedan M, Sherly KB. Synthesis and characterization of nanomesoporous lanthanum aluminate ($LaAlO_3$) for catalytic wet air oxidation of phenol. Emergent Mater. 2020;3:267–77. doi:10.1007/s42247-020-00097-y

9. Rivero-Antúnez P, Morales-Flórez V, Cumbrera FL, Esquivias L. Rietveld analysis and mechanical properties of in situ formed $La-\beta-Al_2O_3/Al_2O_3$ composites prepared by sol-gel method. Ceram Int. 2022;48(17):24462–70. doi:10.1016/j.ceramint.2022.05.058

10. Egorova AV, Belova KG, Animitsa IE, Morkhova YA, Kabanov AA. Effect of zinc doping on electrical properties of $LaAlO_3$ perovskite. Chim Techno Acta. 2021;8(1):20218103. doi:10.15826/chimtech.2020.8.1.03

11. Filonova E, Medvedev D. Recent Progress in the Design, Characterisation and Application of $LaAlO_3$- and $LaGaO_3$-Based Solid Oxide Fuel Cell Electrolytes. Nanomater. 2022;12(12):1991. doi:10.3390/nano12121991

12. Kumar P, Singh S, Gupta I, Kumar V, Singh D. $Er^{3+}$ activated $LaAlO_3$ perovskite phosphor: Crystal structure and down conversion photoluminescent behaviour for optoelectronic devices. Inorg Chem Commun. 2022;141:109578. doi:10.1016/j.inoche.2022.109578

13. Kumar P, Singh S, Gupta I, Kumar V, Singh D. Structural and optical characterization of trivalent samarium-activated $LaAlO_3$ nanocrystalline materials for solid-state lighting. J Mol Struct. 2022;1265:133362. doi:10.1016/j.molstruc.2022.133362

14. Kumar P, Singh S, Gupta I, Kumar V, Singh D. Preparation and luminescence behaviour of perovskite $LaAlO_3:Tb^{3+}$ nanophosphors for innovative displays. Optik. 2022;267:169709. doi:10.1016/j.ijleo.2022.169709

15. Muñoz HJ, Korili SA, Gil A. Progress and Recent Strategies in the Synthesis and Catalytic Applications of Perovskites Based on Lanthanum and Aluminum. Mater. 2022;15(9):3288. doi:10.3390/ma15093288

16. Pechini MP. Method of preparing lead and alkaline earth titanates and niobates and coating method using the same to form a capacitor. United States patent US3330697A. 1967 Jan 7.

17. Negahdari Z, Saberi A, Willert-Porada M. Synthesis and characterization of nanocrystalline microwave dielectric $LaAlO_3$ powder via sucrose method. J Alloys Compd. 2009;485:367–71. doi:10.1016/j.jallcom.2009.05.102

18. Zhang Q, Saito F. Mechanochemical Synthesis of Lanthanum Aluminate by Grinding Lanthanum Oxide with Transition Alumina. J Am Ceram Soc. 2000;83:439–41. doi:10.1111/j.1151-2916.2000.tb01215.x

19. Mizukami F, Maeda K, Watanabe M, Masuda K, Sano T, Kuno K. Preparation of Thermostable High-Surface-Area Aluminas and Properties of the Alumina-Supported Pt Catalysts. Stud Surf Sci Catal. 1991;71:557–68. doi:10.1016/S0167-2991(08)63002-5

20. Li J, Wu Y, Pan Y, Guo J. Influence of citrate-to-nitrate ratio on the thermal behavior and chemical environment of

alumina gel. Ceram Int. 2007;33(5):735–8.
doi:10.1016/j.ceramint.2005.12.011

21. Khamkar KA, Jagadale PN, Kulal SR, Bamane SR, Dhapte VV. Synthesis, characterization and electrical properties of nanostructured LaAlO$_3$ by sol–gel auto combustion method. J Mater Sci Mater Electron. 2013;24(11):4482–7. doi:10.1007/s10854-013-1428-3

22. Silveira IS, Ferreira NS, Souza DN. Structural, morphological and vibrational properties of LaAlO$_3$ nanocrystals produced by four different methods. Ceram Int. 2021;47(19):27748–58. doi:10.1016/j.ceramint.2021.06.201

23. Chandradass J, Balasubramanian M, Kim KH. Synthesis and Characterization of LaAlO$_3$ Nanopowders by Various Fuels. Mater Manuf Process. 2010;25(12):1449–53. doi:10.1080/10426914.2010.508962

24. Belyaninova TV, Siunina LA, Mishenina LN. The sol-gel synthesis of calcium aluminate using various polymerizing agents. Tomsk State Univ J Chem. 2016;4(6):65–72. doi:10.17223/24135542/6/7

25. Aruna ST, Kini NS, Rajam KS. Solution combustion synthesis of CeO$_2$–CeAlO$_3$ nano-composites by mixture-of-fuels approach. Mater Res Bull. 2009;44(4):728–33. doi:10.1016/j.materresbull.2008.09.034

26. Chandradass J, Kim KH. Mixture of fuels approach for the solution combustion synthesis of LaAlO$_3$ nanopowders. Adv Powder Technol. 2010;21:100–5. doi:10.1016/j.apt.2009.10.014

27. Lvov OV, Radishchevskaya NI, Nazarova AYu, Minin RV. Sintez pigmentov na osnove soyedineniy margantsa metodom goreniya rastvorov [Synthesis of pigments based on manganese compounds by combustion solutions]. In: 8th Int. Congr. Energy Fluxes Radiat. Eff. 2022 Oct 2-8; Tomsk, Russia. p. 1351–8. doi:10.56761/EFRE2022.N1-P-010801

28. Sakharov KA, Simonenko EP, Simonenko NP, Vaganova ML, Lebedeva YE, Chaynikova AS, Osin IV, Sorokin OYu, Grashchenkov DV, Sevastyanov VG, Kuznetsov NT, Kablov EN. Glycol-citrate synthesis of fine-grained oxides La$_{2-x}$Gd$_x$Zr$_2$O$_7$ and preparation of corresponding ceramics using FAST/SPS process. Ceram Int. 2018;44(7):7647–55. doi:10.1016/j.ceramint.2018.01.188

29. Jain SR, Adiga KC, Pai Verneker VR. A new approach to thermochemical calculations of condensed fuel-oxidizer mixtures. Combust Flame. 1981;40:71–9. doi:10.1016/0010-2180(81)90111-5

30. Doebelin N, Kleeberg R. Profex: a graphical user interface for the Rietveld refinement program BGMN. J Appl Crystallogr. 2015;48(5):1573–80. doi:10.1107/S1600576715014685

31. Shakirzyanov RI, Volodina NO, Kozlovskiy AL, Zdorovets MV, Shlimas DI, Borgekov DB, Garanin YA. Study of the Structural, Electrical, and Mechanical Properties and Morphological Features of Y-Doped CeO$_2$ Ceramics with Porous Structure. J Compos Sci. 2023;7(10):411. doi:10.3390/jcs7100411

32. Nath D, Singh F, Das R. X-ray diffraction analysis by Williamson-Hall, Halder-Wagner and size-strain plot methods of CdSe nanoparticles- a comparative study. Mater Chem Phys. 2020;239:122021. doi:10.1016/j.matchemphys.2019.122021

33. Roduit N. JMicroVision: Image analysis toolbox for measuring and quantifying components of high-definition images. Version 1.3.4. https://jmicrovision.github.io

34. Matveev AV, Nartova AV, Sankova NN, Okunev AG. DLGRAM cloud service for deep-learning analysis of microscopy images. Microsc Res Tech. 2024;87(5):991–8. doi:10.1002/jemt.24480

35. Yagodina AYu, Mishenina LN. Nitrat-tsitratnyy sintez i issledovaniye svoystv lyuminoforov na osnove ortoalyuminata lantana [Nitrate-citrate synthesis and investigation of the properties of phosphors based on lanthanum orthoaluminate]. Tomsk State Univ J Chem. 2023;29:104-15. Russian. doi:10.17223/24135542/29/10

36. Selyunina LA, Mishenina LN, Slizhov YuG, Kozik VV. Effect of citric acid and ethylene glycol on the formation of calcium aluminate via the sol-gel method. Russ J Inorg Chem. 2013;58:450–5. doi:10.1134/S0036023613040165

37. Yu HF, Guo YM. Effects of heating atmosphere on formation of crystalline citrate-derived LaAlO$_3$ nanoparticles, J Alloys Compd. 2011;509:1984–8. doi:10.1016/j.jallcom.2010.10.109

38. Yu HF, Wang J, Wang SS, Kuo YM. Thermochemical behavior of metallic citrate precursors for the production of pure LaAlO$_3$. J Phys Chem Solids. 2009;70:218–23. doi:10.1016/j.jpcs.2008.10.005

39. Behera SK, Sahu PK, Pratihar SK, Bhattacharyya S. Phase evolution in gel-precipitated LaAlO$_3$ ceramics. J Phys Chem Solids. 2008;69(8):2041–6. doi:10.1016/j.jpcs.2008.02.019

40. Mabelane TS, Koao LF, Motloung SV, Motaung TE, Kroon RE, Mhlongo MR. Effect of annealing period on the structure, morphology, and optical properties of CaAl$_2$O$_4$:0.1% Sm$^{3+}$ prepared by citrate sol-gel method. J Mol Struct. 2022;1260:132751. doi:10.1016/j.molstruc.2022.132751

41. Tian ZQ, Yu HT, Wang ZL. Combustion synthesis and characterization of nanocrystalline LaAlO$_3$ powders. Mater Chem Phys. 2007;106:126–9. doi:10.1016/j.matchemphys.2007.05.027

42. Tsvetkova IN, Shilova OA, Drozdova IA, Gomza YuP. Issledovaniye fraktalnoy struktury gibridnykh fosforosilikatnykh i borosilikatnykh materialov poluchennykh zol-gel metodom [Investigation of the fractal structure of hybrid phosphorosilicate and borosilicate materials obtained by the sol-gel method]. Perspektivnyye materialy. 2011;S13:888–95.